Preprints of the 21st IFAC World Congress (Virtual)
Berlin, Germany, July 12-17, 2020

Manipulability Optimization for Coordinated Motion Control of Multi-arm Space Robots

Ruonan Xu * **Jianjun Luo** * **Mingming Wang** *

* *Research & Development Institute of Northwestern Polytechnical University in Shenzhen, 518057 Shenzhen, China* (e-mail: ruonanxu@mail.nwpu.edu.cn; jjluo@nwpu.edu.cn; mwang@nwpu.edu.cn).

Abstract: By maximizing manipulability, the coordination of multi-arm can be enhanced. In this paper, a method to optimize the manipulability index of cooperative manipulation for a free-floating multi-arm space robot is proposed. Firstly, the manipulability optimization is formulated as a nonlinear optimize problem at position level which is hard to solve online. By redefining constraint equation and manipulability index, it is transformed to a constrained quadratic program problem at velocity level incorporating joint velocity physical limits, which generates joint velocity commands to control the multi-arm to complete predefined tasks. Owing to dynamic coupling effects and closed chain constraints formed by cooperative manipulation, the manipulability index is more complex than that of fixed-base or mobile-base manipulators. Hence, the gradient of the index is approximated by numerical algorithms. Simulations based on a dual-arm space robot model are conducted and the results prove that the proposed method is efficient to optimize the manipulability index.

Keywords: motion control, space robots, multi-arm, cooperative manipulation, manipulability optimization

1. INTRODUCTION

Space robots are playing a vital role in on-orbit service missions (Flores-Abad et al., 2014). Compared with single arm, multi-arm space robots can employ more complex tasks due to its bigger capacity and better stability (Wang et al., 2018). Thus, it has been receiving increasing attention from the robotics research community. When carrying out a cooperative task, multi-arm cooperatively grasp a common object and closed kinematic chains are formed. Due to the closed chain constraints, trajectory planning of arm is usually executed in task space. For control of robotic systems, the desired trajectory needs to be mapped from the task space to the joint space in which the actuators provided their input. Hence, this topic falls within the inverse kinematics control problem.

For redundant manipulator, the inverse kinematics may have infinite solutions for a given primary task, making it possible to choose the best solution for a certain performance index of interest so as to facilitate the kinematic control with high quality (Zhang et al., 2018). A classical method for the inverse kinematics of a redundant manipulator is called the pseudoinverse method minimizing a quadratic function of joint velocities (Whitney, 1969). However, this method cannot handle the kinematic singularity problems (Klein and Huang, 1983, Baillieul et al., 1984). To deal with such problems, a damped least-squared inverse of the Jacobian matrix was proposed by Wampler (1986). Furthermore, gradient projection technique utilizing the null space of the Jacobian matrix has been widely implemented to incorporate an extra performance index into the control, such as joint limit avoidance (Liegeois, 1977), manipulability indices (Yoshikawa, 1984, Chiu, 1987, Bayle et al., 2003). Note that most of the aforementioned methods and techniques are based on the pseudoinverse-type formulations and are difficult to incorporate inequality constraints.

More recently, quadratic programming (QP) has been examined as an efficient method owing to the capability of dealing with different constraints and performance indices in a unified manner. Among such performance indices, manipulability of arm has been extensively studied, which is related to the singularities of the Jacobian matrix. Zhang et al. (2016) proposed a novel QP-based refined manipulability-maximizing (ReMM) scheme for coordinated motion planning and control of a physically constrained wheeled mobile redundant manipulator. In Jin et al. (2017), the manipulability optimization scheme was formulated as a constrained QP and a dynamic neural network with rigorously provable convergence was constructed to solve such a problem online. Dufour and Suleiman (2017) integrated the manipulability index into inverse kinematics using approximated derivatives and obstacle avoidance had also been considered.

To our knowledge the manipulability optimization of cooperative manipulation of free-floating multi-arm space robots has not been demonstrated so far and the purpose of this paper is to accomplish this. By maximizing manipulability, not only the singularity can be avoidance,

but also the coordinated performance of multi-arm can be enhanced. However, the manipulability index of free floating closed chain systems are more complex than that of fixed-base or mobile-base manipulators owing to dynamic coupling effects and closed chain constraints. In this paper, task compatibility of multi-arm cooperative manipulation is used as a performance measure of the arms's manipulability. Further, manipulability optimization is transformed from a nonlinear problem to a QP problem in velocity level. The gradient of the manipulability index which is hard to solve analytically is approximated with numerical algorithms.

This paper is organized in the following manner. Section 2 systematically formulates the kinematics and manipulability index of cooperative manipulation of free-floating multi-arm space robots. The manipulability optimization is given as a nonlinear problem. In Section 3, the nonlinear problem is reformulated as a constrained QP problem and gradient of the nonlinear performance index is approximated with numerical algorithms. In Section 4, simulations are conducted to show that the proposed methods are indeed useful for manipulability optimization. The conclusive remarks are listed in Section 5.

2. PROBLEM FORMULATION

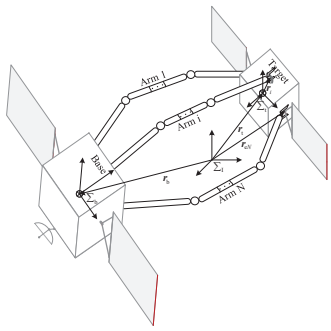

Fig. 1. Schematic diagram of cooperative manipulation of a multi-arm space robot.

Fig. 1 illustrates a cooperative system with N arms manipulating a common object. Consider each arm with n_k DOF attached to a free-floating base satellite, and whose end-effector acts in an m-dimensional task space with $m \leq n_k$. In the following, kinematics and manipulability analysis for the closed chain system are presented for problem formulation.

2.1 Closed Chain Kinematics

The Cartesian coordinate $\boldsymbol{x}_\mathrm{e} = \left[\, \boldsymbol{x}_{\mathrm{e}1}^\mathrm{T} \ \cdots \ \boldsymbol{x}_{\mathrm{e}N}^\mathrm{T} \,\right]^\mathrm{T} \in \mathbb{R}^{mN}$ of end-effectors in the workspace can be described as a nonlinear mapping

$$\boldsymbol{x}_\mathrm{e} = \boldsymbol{f}\left(\boldsymbol{x}_\mathrm{b}, \boldsymbol{\theta}\right) \tag{1}$$

where the mapping $\boldsymbol{f}(\cdot)$ carries mechanical and geometrical information of a space robot, while $\boldsymbol{x}_\mathrm{b} = [\, \boldsymbol{r}_b^\mathrm{T} \ \boldsymbol{q}_b^\mathrm{T} \,]^\mathrm{T} \in \mathbb{R}^7$ and $\boldsymbol{\theta} = \left[\, \boldsymbol{\theta}_1^\mathrm{T} \ \cdots \ \boldsymbol{\theta}_N^\mathrm{T} \,\right]^\mathrm{T} \in \mathbb{R}^{\sum_{k=1}^{N} n_k}$ denote the base and the joint variables, respectively. $\boldsymbol{r}_\mathrm{b} \in \mathbb{R}^3$ is the position of the base and $\boldsymbol{q}_b \in \mathbb{R}^4$ is a quaternion which present the attitude of the base. Computing time derivations on both sides of Eq. (1), we have

$$\dot{\boldsymbol{x}}_\mathrm{e} = \boldsymbol{J}_\mathrm{b}\dot{\boldsymbol{x}}_\mathrm{b} + \boldsymbol{J}_\mathrm{m}\dot{\boldsymbol{\theta}} \tag{2}$$

where $\boldsymbol{J}_\mathrm{b} \in \mathbb{R}^{mN\times m}$ and $\boldsymbol{J}_\mathrm{m} \in \mathbb{R}^{mN\times\sum_{k=1}^{N} n_k}$ being the Jacobian matrices for the base and for the arms, respectively. And $\dot{\boldsymbol{x}}_\mathrm{b} = [\, \boldsymbol{v}_b^\mathrm{T} \ \boldsymbol{\omega}_b^\mathrm{T} \,]^\mathrm{T} \in \mathbb{R}^6$ includes the linear velocity and angular velocity of the base.

Assuming that the initial linear and angular momentums are equal to zeros and no external force or torque acts on the system, the momentum conservation equations of the free-floating closed chain system can be preserved as follows

$$\boldsymbol{H}_\mathrm{bc}\dot{\boldsymbol{x}}_\mathrm{b} + \boldsymbol{H}_\mathrm{mc}\dot{\boldsymbol{\theta}} = \boldsymbol{0} \tag{3}$$

where $\boldsymbol{H}_\mathrm{bc} \in \mathbb{R}^{m\times m}$ and $\boldsymbol{H}_\mathrm{mc} \in \mathbb{R}^{m\times\sum_{k=1}^{N} n_k}$ are the base inertia and coupling inertia matrices, respectively. So the relationship between the base velocity and the joint angular velocity is expressed as

$$\dot{\boldsymbol{x}}_\mathrm{b} = -\boldsymbol{H}_\mathrm{bc}^{-1}\boldsymbol{H}_\mathrm{mc}\dot{\boldsymbol{\theta}} \tag{4}$$

Substituting Eq. (4) into Eq. (2) yields

$$\dot{\boldsymbol{x}}_\mathrm{e} = \left(\boldsymbol{J}_\mathrm{m} - \boldsymbol{J}_\mathrm{b}\boldsymbol{H}_\mathrm{bc}^{-1}\boldsymbol{H}_\mathrm{mc}\right)\dot{\boldsymbol{\theta}} = \boldsymbol{J}\dot{\boldsymbol{\theta}} \tag{5}$$

The velocity constraints due to the closed kinematic chain, which expresses the velocity relationship between the target and the end-effectors, are given through a matrix $\boldsymbol{G} \in \mathbb{R}^{m\times mN}$ as follows

$$\boldsymbol{G}^\mathrm{T}\dot{\boldsymbol{x}}_\mathrm{t} = \dot{\boldsymbol{x}}_\mathrm{e} \tag{6}$$

where $\boldsymbol{x}_\mathrm{t} \in \mathbb{R}^m$ denotes the target variable, $\boldsymbol{G}$ is the so-called grasp matrix presented as

$$\boldsymbol{G} = \begin{bmatrix} \boldsymbol{I} & \boldsymbol{0} & \cdots & \boldsymbol{I} & \boldsymbol{0} \\ \boldsymbol{r}_1^\times & \boldsymbol{I} & & \boldsymbol{r}_N^\times & \boldsymbol{I} \end{bmatrix}$$

where $\boldsymbol{I}$ and $\boldsymbol{0}$ denote identify and null matrices of appropriate dimensions, respectively. $\boldsymbol{r}_i$ is the grasp point position respect to target center, and $\boldsymbol{a}^\times$ is a skew symmetrical matrix, which can be calculated for $\boldsymbol{a} = [a_x, a_y, a_z]^\mathrm{T}$ as

$$\boldsymbol{a}^\times = \begin{bmatrix} 0 & -a_z & a_y \\ a_z & 0 & -a_x \\ -a_y & a_x & 0 \end{bmatrix}$$

From Eqs. (5) and (6), the kinematic relationship at velocity level for task is given as

$$\dot{\boldsymbol{\theta}} = \boldsymbol{J}^+\boldsymbol{G}^\mathrm{T}\dot{\boldsymbol{x}}_\mathrm{t} \tag{7}$$

where $\boldsymbol{J}^+$ is the pseudoinverse of matrix.

2.2 Cooperative Manipulation Manipulability

It is well-known that the *manipulability measure* introduced by Yoshikawa (1985) is widely used in manipulator performance measures. It is applied to describe the volume of *manipulability ellipsoids* which depict the manipulability of arm in all directions. Giving the velocity limits of $\dot{\theta}_i^j$ as

$$\left|\dot{\theta}_i^j\right| \leq \dot{\theta}_{i,max}^j, i = 1, \cdots, N, j = 1, \cdots, n_k \tag{8}$$

where $\dot{\theta}_{i,\max}^j$ is the bound of the j-th joint velocity for arm i. Consider the weight matrix $\boldsymbol{W}$, where $\boldsymbol{W}$ =

$diag\left(\left[\frac{1}{\dot{\theta}^1_{1,max}},\cdots,\frac{1}{\dot{\theta}^{n_N}_{N,max}}\right]\right)$, a suitable scaling of the joint velocity is defined as $\tilde{\dot{\boldsymbol{\theta}}}$, that is

$$\tilde{\dot{\boldsymbol{\theta}}} = \boldsymbol{W}\dot{\boldsymbol{\theta}} \tag{9}$$

The velocity manipulability ellipsoid is defined as the primage of the unit sphere in the space of the scaled joint velocity

$$\tilde{\dot{\boldsymbol{\theta}}}^{\mathrm{T}}\tilde{\dot{\boldsymbol{\theta}}} \leq 1 \tag{10}$$

which, under the mapping of Eqs. (7) and (9), is given by

$$\dot{\boldsymbol{x}}_{\mathrm{t}}^{\mathrm{T}}\boldsymbol{G}\boldsymbol{J}^{+\mathrm{T}}\boldsymbol{W}^{\mathrm{T}}\boldsymbol{W}\boldsymbol{J}^{+}\boldsymbol{G}^{\mathrm{T}}\dot{\boldsymbol{x}}_{\mathrm{t}} \leq 1 \tag{11}$$

The *manipulability measure* represented by a scale value m^w is given as a quantitative measure for the local manipulability of the arms, which is defined as

$$m^w = \sqrt{\det((\boldsymbol{G}\boldsymbol{J}^{+\mathrm{T}}\boldsymbol{W}^{\mathrm{T}}\boldsymbol{W}\boldsymbol{J}^{+}\boldsymbol{G}^{\mathrm{T}})^{-1})} \tag{12}$$

Additionally, the transmission ratio along a particular direction called *task compatibility* (Chiu, 1988) is used to represent the manipulability of arm in a desired direction. To describe the task compatibility of multi-arm in a desired task direction, a unit velocity $\boldsymbol{u}$ is used, which represents the direction of a task. Then we have

$$\dot{\boldsymbol{x}}_{\mathrm{t}} = s\boldsymbol{u} \tag{13}$$

where the scale value s denotes the velocity transmission ratio of $\dot{\boldsymbol{x}}_{\mathrm{t}}$ in the direction of $\boldsymbol{u}$. Therefore, s has to satisfy the following inequations substituting Eq. (13) into Eq. (11)

$$s^2\boldsymbol{u}^{\mathrm{T}}\boldsymbol{G}\boldsymbol{J}^{+\mathrm{T}}\boldsymbol{W}^{\mathrm{T}}\boldsymbol{W}\boldsymbol{J}^{+}\boldsymbol{G}^{\mathrm{T}}\boldsymbol{u} \leq 1 \tag{14}$$

From Eq. (14), the maximum value m^s of velocity on the desired direction $\boldsymbol{u}$ is given as follows

$$m^s = \left(\boldsymbol{u}^{\mathrm{T}}\boldsymbol{G}\boldsymbol{J}^{+\mathrm{T}}\boldsymbol{W}^{\mathrm{T}}\boldsymbol{W}\boldsymbol{J}^{+}\boldsymbol{G}^{\mathrm{T}}\boldsymbol{u}\right)^{-1/2} \tag{15}$$

2.3 Optimization Problem Formulation

Based on the above analysis, the inverse kinematics of multi-arm cooperative manipulation with manipulability optimality considered can be formulated as a constrained optimization problem

$$\min_{\boldsymbol{\theta}} \; -m(\boldsymbol{x}) \tag{16a}$$

$$s.t. \;\; \boldsymbol{f}(\boldsymbol{x}) = \boldsymbol{x}_{\mathrm{e}}^{\mathrm{d}} \tag{16b}$$

where $\boldsymbol{x} = [\,\boldsymbol{x}_{\mathrm{b}}^{\mathrm{T}} \;\; \boldsymbol{\theta}^{\mathrm{T}}\,]^{\mathrm{T}}$ and $\boldsymbol{x}_{\mathrm{e}}^{\mathrm{d}}$ is the desired pose of end-effectors. $m(\boldsymbol{x})$ is a manipulability index chosen as m^w or m^s for different task requirements. Eq. (16b) represents the forward kinematic equation including the closed chain constraints.

In this optimization problem, $m(\boldsymbol{x})$ and $\boldsymbol{f}(\boldsymbol{x})$ are related not only to optimization variable $\boldsymbol{\theta}$, but also to the coupling base variable $\boldsymbol{x}_{\mathrm{b}}$. But, the position level relationship between $\boldsymbol{x}_{\mathrm{b}}$ and θ is hard to obtain owing to the nonholonomic constraint of free-floating space robots. Additionally, $m(\boldsymbol{x})$ and $\boldsymbol{f}(\boldsymbol{x})$ are also nonlinear. Thus, the solution of $\boldsymbol{\theta}$ in Eq. (16) becomes a challenging problem.

3. REFORMULATION AS A CONSTRAINED QP

By redefining the constraint equation and performance index, the nonlinear optimization problem is transformed into a constrained QP problem at velocity level. Besides, the physical constraint of joint velocity is incorporated.

3.1 Constraint Equation: Velocity-Level

Owing to the strong nonlinearity of the position level kinematic equation, the velocity level one is used to represent the constraint equation (16b) as follows

$$\boldsymbol{J}\dot{\boldsymbol{\theta}} = \dot{\boldsymbol{x}}_{\mathrm{e}}^{\mathrm{d}} + \boldsymbol{\Lambda}(\boldsymbol{x}_{\mathrm{e}}^{\mathrm{d}} - \boldsymbol{f}(\boldsymbol{x})) \tag{17}$$

where $\boldsymbol{\Lambda} \in \mathbb{R}^{mN\times mN}$ is a positive definite matrix. Note that Eq. (17) is asymptotically equivalent to $\boldsymbol{f}(\boldsymbol{x}) = \boldsymbol{x}_{\mathrm{e}}^{\mathrm{d}}$ because of $\boldsymbol{f}(\boldsymbol{x})$ exponentially converging to $\boldsymbol{x}_{\mathrm{e}}^{\mathrm{d}}$ over time.

When multi-arm manipulating a common object cooperatively, the desired position and velocity of the end-effectors can be derived as follows

$$\boldsymbol{x}_{\mathrm{e}}^{\mathrm{d}} = {}^{\mathrm{t}}\boldsymbol{T}_{\mathrm{e}}^{\mathrm{T}}\boldsymbol{x}_{\mathrm{t}}^{\mathrm{d}} \tag{18a}$$

$$\dot{\boldsymbol{x}}_{\mathrm{e}}^{\mathrm{d}} = \boldsymbol{G}^{\mathrm{T}}\dot{\boldsymbol{x}}_{\mathrm{t}}^{\mathrm{d}} \tag{18b}$$

where $\boldsymbol{x}_{\mathrm{t}}^{\mathrm{d}}$ is the desired task variable of target and ${}^{\mathrm{t}}\boldsymbol{T}_{\mathrm{e}}$ represents the transformation matrix of the end-effectors relative to the target. Substituting Eqs. (18a) and (18b) into (17), the constraint equation (16b) is more explicitly defined by

$$\boldsymbol{J}\dot{\boldsymbol{\theta}} = \boldsymbol{G}^{\mathrm{T}}\dot{\boldsymbol{x}}_{\mathrm{t}}^{\mathrm{d}} + \boldsymbol{\Lambda}({}^{\mathrm{t}}\boldsymbol{T}_{\mathrm{e}}^{\mathrm{T}}\boldsymbol{x}_{\mathrm{t}}^{\mathrm{d}} - \boldsymbol{f}(\boldsymbol{x})) \tag{19}$$

3.2 Performance Index: Gradient Maximization

In order to transform Eq. (16) into a QP problem, the performance index (16a) is reformulated by using the gradient of $m(\boldsymbol{x})$ which is a function of $\dot{\boldsymbol{\theta}}$. As $m(\boldsymbol{x}^k) = m(\boldsymbol{x}^{k-1}) + \dot{m}(\boldsymbol{x}^{k-1})\mathrm{d}_{\mathrm{time}}$, where $\mathrm{d}_{\mathrm{time}}$ is sampling time and k and $k-1$ is two adjacent sampling points, by maximizing $\dot{m}(\boldsymbol{x}^{k-1})$, the maximization of the manipulability $m(\boldsymbol{x}^k)$ can also be achieved.

Based on the above discussion, the gradient of $m(\boldsymbol{x})$ is calculated as

$$\dot{m}(\boldsymbol{x}) = \frac{\partial m}{\partial \boldsymbol{x}_{\mathrm{b}}}\dot{\boldsymbol{x}}_{\mathrm{b}} + \frac{\partial m}{\partial \boldsymbol{\theta}}\dot{\boldsymbol{\theta}} \tag{20}$$

For free-floating space robots, the dynamic coupling effects between the base and arms can be represent by Eq (4) at velocity level. Substituting Eq. (4) into Eq. (20), directly we have

$$\dot{m}(\boldsymbol{x}) = \left(\frac{\partial m}{\partial \boldsymbol{\theta}} - \frac{\partial m}{\partial \boldsymbol{x}_{\mathrm{b}}}\boldsymbol{H}_{\mathrm{bc}}^{-1}\boldsymbol{H}_{\mathrm{mc}}\right)\dot{\boldsymbol{\theta}} \tag{21}$$

By incorporating one extra term $\frac{1}{2}\dot{\boldsymbol{\theta}}^{\mathrm{T}}\boldsymbol{W}\dot{\boldsymbol{\theta}}$ to regulate the kinematic energy consumption and considering the physical limits of the arms, the manipulability optimization in velocity level is reformulated as

$$\min_{\dot{\boldsymbol{\theta}}} \; \frac{1}{2}\dot{\boldsymbol{\theta}}^{\mathrm{T}}\boldsymbol{W}\dot{\boldsymbol{\theta}} - \alpha\left(\frac{\partial m}{\partial \boldsymbol{\theta}} - \frac{\partial m}{\partial \boldsymbol{x}_{\mathrm{b}}}\boldsymbol{H}_{\mathrm{bc}}^{-1}\boldsymbol{H}_{\mathrm{mc}}\right)\dot{\boldsymbol{\theta}} \tag{22a}$$

$$s.t. \quad \boldsymbol{J}\dot{\boldsymbol{\theta}} = \boldsymbol{G}^{\mathrm{T}}\dot{\boldsymbol{x}}_{\mathrm{t}}^{\mathrm{d}} + \boldsymbol{\Lambda}({}^{\mathrm{t}}\boldsymbol{T}_{\mathrm{e}}^{\mathrm{T}}\boldsymbol{x}_{\mathrm{t}}^{\mathrm{d}} - \boldsymbol{f}(\boldsymbol{x})) \tag{22b}$$

$$\dot{\boldsymbol{\theta}}^{-} \leq \dot{\boldsymbol{\theta}} \leq \dot{\boldsymbol{\theta}}^{+} \tag{22c}$$

where α is a weight coefficient and $\dot{\boldsymbol{\theta}}^{-}$ and $\dot{\boldsymbol{\theta}}^{+}$ are the lower and the upper bounds of $\dot{\boldsymbol{\theta}}$, respectively. Note that

the nonlinear optimization problem is transformed into a constrained QP problem. The calculated method for the gradient of m in Eq. (22a) is given in the following section.

3.3 Gradient of Manipulability Index

As the attitude of base is describe by a quaternion, $\frac{\partial m}{\partial \boldsymbol{x}_\mathrm{b}}$ is computed as $\frac{\partial m}{\partial \boldsymbol{x}_\mathrm{b}} = \left[\frac{\partial m}{\partial \boldsymbol{r}_\mathrm{b}} \ \frac{1}{2}\frac{\partial m}{\partial \boldsymbol{q}_\mathrm{b}}\boldsymbol{Q}(\boldsymbol{q}_\mathrm{b})\right]$. Defining $\boldsymbol{q}_b = [\,\eta \ \boldsymbol{q}^\mathrm{T}\,]^\mathrm{T}$, $\boldsymbol{Q}(\boldsymbol{q}_\mathrm{b})$ is expressed by

$$\boldsymbol{Q}(\boldsymbol{q}_\mathrm{b}) = \begin{bmatrix} -\boldsymbol{q}^\mathrm{T} \\ \eta\boldsymbol{I} - \boldsymbol{q}^\times \end{bmatrix}$$

Compared with fixed-base or mobile-base manipulators, the manipulability of free-floating closed chain systems is more complex. From Eqs. (12) and (15), it can be noted that $m(\boldsymbol{x})$ are related not only to Jacobian and grasp matrices, but also to inertia matrices. Hence, it is hard to find a direct analytical relationship between $m(\boldsymbol{x})$ and $\boldsymbol{\theta}$ to calculate the gradient of $m(\boldsymbol{x})$. Thus, it is approximated numerically by

$$\left(\frac{\partial m}{\partial \boldsymbol{r}_\mathrm{b}}\right)_k = \frac{m\left(\boldsymbol{x} + \delta r_\mathrm{b}^k \boldsymbol{I}_k\right) - m\left(\boldsymbol{x} - \delta r_\mathrm{b}^k \boldsymbol{I}_k\right)}{2\delta r_\mathrm{b}^k} \tag{23a}$$

$$\left(\frac{\partial m}{\partial \boldsymbol{q}_\mathrm{b}}\right)_k = \frac{m\left(\boldsymbol{x} + \delta q_\mathrm{b}^k \boldsymbol{I}_{3+k}\right) - m\left(\boldsymbol{x} - \delta q_\mathrm{b}^k \boldsymbol{I}_{3+k}\right)}{2\delta q_\mathrm{b}^k} \tag{23b}$$

$$\left(\frac{\partial m}{\partial \boldsymbol{\theta}}\right)_k = \frac{m\left(\boldsymbol{x} + \delta \theta_i^j \boldsymbol{I}_{7+k}\right) - m\left(\boldsymbol{x} - \delta \theta_i^j \boldsymbol{I}_{7+k}\right)}{2\delta \theta_i^j} \tag{23c}$$

where $\left(\frac{\partial m}{\partial \boldsymbol{r}_\mathrm{b}}\right)_k, k = 1,2,3$, $\left(\frac{\partial m}{\partial \boldsymbol{q}_\mathrm{b}}\right)_k, k = 1,2,3,4$ and $\left(\frac{\partial m}{\partial \boldsymbol{\theta}}\right)_k, k = 1, \cdots, \sum_{k=1}^{N} n_k$ are the k^{th} element of vector $\frac{\partial m}{\partial \boldsymbol{r}_\mathrm{b}}$, $\frac{\partial m}{\partial \boldsymbol{q}_\mathrm{b}}$ and $\frac{\partial m}{\partial \boldsymbol{\theta}}$, respectively, δ is a small increment and $\boldsymbol{I}_{(\cdot)} \in \mathbb{R}^{7+\sum_{k=1}^{N} n_k}$, for any a, $\boldsymbol{I}_a$ is given as follows

$$\boldsymbol{I}_a = [0 \ \ldots \ \underset{\uparrow}{1} \ \ldots \ 0]^\mathrm{T}$$
$$a$$

Using these formulations, it is then easy to compute the performance index of Eq. (22) since only the manipulability index of different configurations is computed.

4. SIMULATION

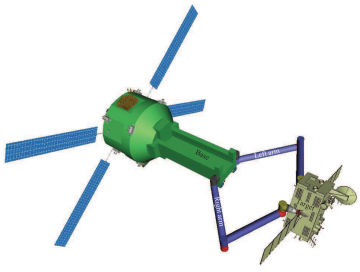

Fig. 2. Simulation model: a dual-arm space robot

In this section, simulations are conducted on a dual-arm space robot shown in Fig. 2 with the kinematic and dynamic parameters summarized in Table 1 to demonstrate the effectiveness of the proposed manipulability optimization scheme.

Table 1. Kinematic and dynamic parameters of space robot and target

robot	base	left arm (right arm) modified DH							target
		j1	j2	j3	j4	j5	j6	j7	
a_i,m	–	0.8	0	0	0	0	0	0	–
α_i,deg	–	-90(90)	-90(90)	90(-90)	90(-90)	90(-90)	-90(90)	90(-90)	–
b_i,m	–	0.856	0.168	1.450	0.168	1.290	0.168	0.084	–
q,deg	–	θ_i^1	θ_i^2	θ_i^3	θ_i^4	$\theta_i^5 - 90$	$\theta_i^6 - 90$	θ_i^7	–
m,kg	400	3	8	2	6	2	2	4	100
I_{xx},kg·m^2	128	0.0041	1.3824	0.0047	0.8712	0.0047	0.0047	0.0645	10
I_{yy},kg·m^2	340	0.0041	0.0256	0.0064	0.0192	0.0064	0.0047	0.0645	20
I_{zz},kg·m^2	340	0.0096	1.3824	0.0047	0.8712	0.0047	0.0064	0.0128	20

The pose of the base in inertia frame is set as $\boldsymbol{r}_\mathrm{b} = [\,0 \ 0 \ 0\,]^\mathrm{T}$ m and $\boldsymbol{q}_\mathrm{b} = [\,1 \ 0 \ 0 \ 0\,]^\mathrm{T}$. The grasp points e_1 and e_2 for the end-effectors are described by

$${}^\mathrm{t}\boldsymbol{T}_{\mathrm{e}1} = \begin{bmatrix} 0 & 0 & 1 & -0.5 \\ 0 & 1 & 0 & 0.4 \\ -1 & 0 & 0 & 0 \\ 0 & 0 & 0 & 1 \end{bmatrix}, \ {}^\mathrm{t}\boldsymbol{T}_{\mathrm{e}2} = \begin{bmatrix} 0 & 0 & 1 & -0.5 \\ 0 & -1 & 0 & -0.4 \\ 1 & 0 & 0 & 0 \\ 0 & 0 & 0 & 1 \end{bmatrix}$$

Fig. 3 shows the manipulability ellipsoid of the arms in different configurations, and the corresponding manipulability m^w and m^s as functions of the robotic arms stretching. From Fig. 3, it can be noted that the manipulability of the arms varies with the change of the configurations. The zero value of manipulability measure means that the robot passes a singularity configuration, which is shown in Fig. 3(a). In the following, self-motion and trajectory tracking with manipulability optimization are demonstrated to verify the effectiveness of the proposed method.

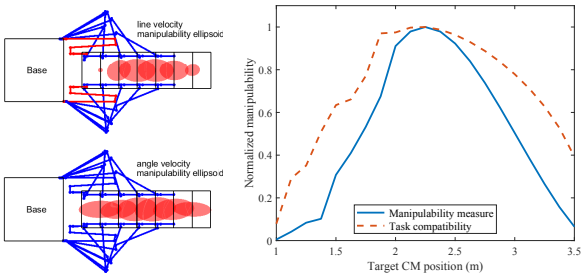

(a) (b)

Fig. 3. Manipulability analysis for the dual-arm cooperative manipulation. (a) Manipulability Ellipsoids. (b) Normalized manipulability index.

4.1 Manipulability Optimization Via self motion

Giving the pose of target in Cartesian coordinate as $\boldsymbol{r}_\mathrm{t} = [\,2.5 \ 0 \ 0\,]^\mathrm{T}$ m and $\boldsymbol{q}_\mathrm{t} = [\,1 \ 0 \ 0 \ 0\,]^\mathrm{T}$. Fig. 4 shows the motion trajectories of space robot's base and arms while the manipulability optimization with the end-effectors fixed in Cartesian space. The initial configuration is given by minimizing a quadratic function of joint angles. Compared with that of the initial configuration, m^w of the optimized configuration is increased by 76.76%, which means that the proposed manipulability optimization method is effective.

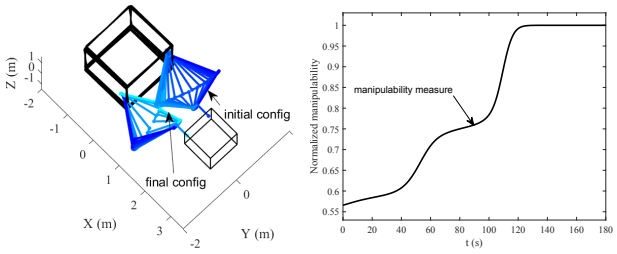

(a) (b)

Fig. 4. Simulation results for the manipulability optimization of the closed system via self motion. (a) Motion trajectories. (b) Normalized manipulability index.

4.2 Manipulability Optimization in trajectory Tracking

In this section, manipulability optimization is conducted to track a circular trajectory and a sinusoidal trajectory with joint velocity constraints. The velocity constraints are given as $|\dot{\theta}_i^j| \leq 0.5$ rad/s. The task compatibility is important for arms to enhance the manipulability along the special task direction while tracking a trajectory. Hence, m^s in Eq. (15) is used in this section as the manipulability index.

The circular trajectory of the target is given as follows

$$\begin{cases} \boldsymbol{r}_{\mathrm{t}} = [\,1.7 + 0.3\cos(\frac{\pi}{5}t),\ 0.3\sin(\frac{\pi}{5}t),\ 0\,]^{\mathrm{T}} \\ \boldsymbol{q}_{\mathrm{t}} = [\,1,\ 0,\ 0,\ 0\,]^{\mathrm{T}} \end{cases}$$

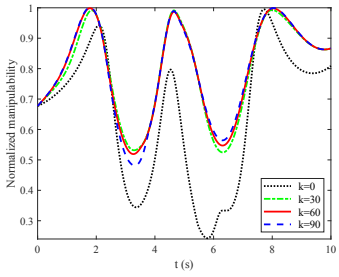

Fig. 5. Normalized manipulability index evolution while tracking a circular trajectory for different k.

Fig. 5 shows the impact of weight coefficient α to the manipulability optimization while tracking the given circular trajectory. Among a appropriate range, the influence of α to manipulability index is little. And α is chosen as 35 for the circular trajectory and 45 for the sinusoidal trajectory in the simulation.

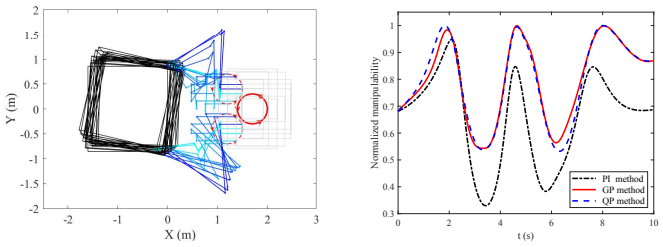

(a) (b)

Fig. 6. Simulation results on motion trajectories and manipulability index for the manipulability optimization of the closed chain system tracking a circular trajectory. (a) Motion trajectories. (b) Normalized manipulability index for different methods.

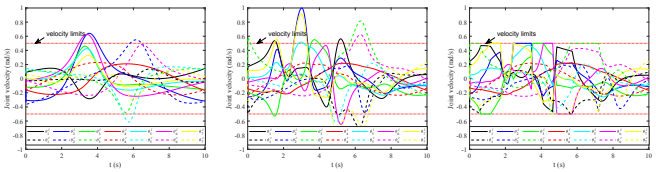

(a) (b) (c)

Fig. 7. Joint velocities of tracking a circular trajectory for different methods. (a) Pseudoinverse method. (b) Gradient projection method. (c) Quadratic programming method.

The sinusoidal trajectory of the target is given as follows

$$\begin{cases} \boldsymbol{r}_{\mathrm{t}} = [\,1.5 + \frac{1}{12}t,\ 0.5\sin(\frac{\pi}{6}t),\ 0\,]^{\mathrm{T}} \\ \boldsymbol{q}_{\mathrm{t}} = [\,1,\ 0,\ 0,\ 0\,]^{\mathrm{T}} \end{cases}$$

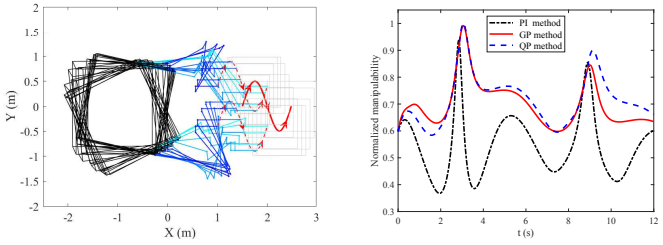

(a) (b)

Fig. 8. Simulation results on motion trajectories and manipulability index for the manipulability optimization of the closed chain system tracking a sinusoidal trajectory. (a) Motion trajectories. (b) Normalized manipulability index for different methods.

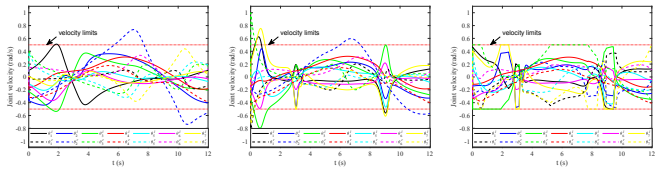

(a) (b) (c)

Fig. 9. Joint velocities of tracking a sinusoidal trajectory for different methods. (a) Pseudoinverse method. (b) Gradient projection method. (c) Quadratic programming method.

The motion trajectories of the space robotic system with manipulability optimization for tracking a circular trajectory and a sinusoidal trajectory are illustrated in Figs. 6(a) and 8(a), respectively. Figs. 7(a) and 7(b) show the corresponding normalized manipulability index evolution of the proposed QP method comparing with two classical inverse kinematic solver method, pseudoinverse method (Whitney, 1969) and gradient projection technique (Liegeois, 1977). The pseudoinverse method can minimize the quadratic function of joint velocities. Gradient projection technique can maximize the manipulability index by using the null-space of Jacobian matrix. The joint velocities while tracking the designed circular trajectory and sinusoidal trajectory for the three method are shown in Figs. 7 and 9, respectively. It can be noted that the proposed method has a good effect on manipulability optimization while keeping the joint velocity constraints.

5. CONCLUSION

This paper has proposed a manipulability optimization method for multi-arm space robots cooperative manipulation. The optimization problem is solved at velocity level, which generates the coordinated velocity control commands to perform a predefined task. Simulation results have proven that this method is effective to increase the manipulability index along the given task trajectories.

The results of this method can be used in cooperative motion control when a space robot's multi-arm cooperatively manipulating a common object. Future work will take the joint angle physical limits and obstacle avoidance problem into consideration.

ACKNOWLEDGEMENTS

This work was Supported by "The National Natural Science Foundation of China (Grant No. 61973256, 61690210 and 61690211)", and the Innovation Foundation for Doctor Dissertation of Northwestern Polytechnical University under Grant Number CX201903.

REFERENCES

Baillieul, J., Hollerbach, J., and Brockett, R. (1984). Programming and control of kinematically redundant manipulators. In *The 23rd IEEE Conference on Decision and Control*, 768–774. IEEE.

Bayle, B., Fourquet, J.Y., and Renaud, M. (2003). Manipulability of wheeled mobile manipulators: Application to motion generation. *The International Journal of Robotics Research*, 22(7-8), 565–581.

Chiu, S.L. (1988). Task compatibility of manipulator postures. *The International Journal of Robotics Research*, 7(5), 13–21.

Chiu, S. (1987). Control of redundant manipulators for task compatibility. In *Proceedings. 1987 IEEE International Conference on Robotics and Automation*, volume 4, 1718–1724. IEEE.

Dufour, K. and Suleiman, W. (2017). On integrating manipulability index into inverse kinematics solver. In *2017 IEEE/RSJ International Conference on Intelligent Robots and Systems (IROS)*, 6967–6972. IEEE.

Flores-Abad, A., Ma, O., Pham, K., and Ulrich, S. (2014). A review of space robotics technologies for on-orbit servicing. *Progress in Aerospace Sciences*, 68, 1–26.

Jin, L., Li, S., La, H.M., and Luo, X. (2017). Manipulability optimization of redundant manipulators using dynamic neural networks. *IEEE Transactions on Industrial Electronics*, 64(6), 4710–4720.

Klein, C.A. and Huang, C.H. (1983). Review of pseudoinverse control for use with kinematically redundant manipulators. *IEEE Transactions on Systems, Man, and Cybernetics*, (2), 245–250.

Liegeois, A. (1977). Automatic supervisory control of the configuration and behaviour of multibody mechanisms. *IEEE Transactions on systems, man and cybernetics*, 7(12), 868–871.

Wampler, C.W. (1986). Manipulator inverse kinematic solutions based on vector formulations and damped least-squares methods. *IEEE Transactions on Systems, Man, and Cybernetics*, 16(1), 93–101.

Wang, M., Luo, J., Yuan, J., and Walter, U. (2018). Coordinated trajectory planning of dual-arm space robot using constrained particle swarm optimization. *Acta Astronautica*, 146, 259–272.

Whitney, D.E. (1969). Resolved motion rate control of manipulators and human prostheses. *IEEE Transactions on man-machine systems*, 10(2), 47–53.

Yoshikawa, T. (1984). Analysys and control of robot manipulators with redundancy. robotic research. *The First International Syposium, 1984*, 735–747.

Yoshikawa, T. (1985). Manipulability of robotic mechanisms. *The international journal of Robotics Research*, 4(2), 3–9.

Zhang, Y., Li, S., and Zhou, X. (2018). Recurrent-neural-network-based velocity-level redundancy resolution for manipulators subject to a joint acceleration limit. *IEEE Transactions on Industrial Electronics*, 66(5), 3573–3582.

Zhang, Y., Yan, X., Chen, D., Guo, D., and Li, W. (2016). Qp-based refined manipulability-maximizing scheme for coordinated motion planning and control of physically constrained wheeled mobile redundant manipulators. *Nonlinear Dynamics*, 85(1), 245–261.